Electrostatic-Induced Interfacial Assembly of Enzymes with Nanosheets: Controlled Orientation and Optimized Activity

Zhe An, Jing He, Shan Lu, and Lan Yang
State Key Laboratory of Chemical Resource Engineering,
Beijing University of Chemical Technology, Beijing 100029, People's Republic of China

DOI 10.1002/aic.12147
Published online March 29, 2010 in Wiley Online Library (wileyonlinelibrary.com).

In this work, an electrostatic-induced interfacial assembly of porcine pancreatic lipase (PPL) with the nanosheets of layered double hydroxide (LDHNSs) is designed to rationally control the orientation of bound PPL. The PPL orientation in the bidimensional confinement spacing alters relying on the PPL loading, with the majority of active sites facing the LDH layer at low PPL loading and facing the adjacent protein molecule at high PPL loading. The biocatalytic activity of the bound PPL significantly depends on its orientation. Remarkable enhancement of the bio-activity has been observed when the PPL/LDHNSs mass ratio is less than 9, and a maximum activity is met with at PPL/LDHNSs = 0.5. In addition, the thermal stability of PPL-LDHNSs bioactivity has been obviously improved in comparison with soluble PPL. © 2010 American Institute of Chemical Engineers *AIChE J,* 56: 2677–2686, 2010
Keywords: protein adsorption, surface recognition, electrostatic assembly, protein orientation, nanosheets, layered double hydroxide

Introduction

Widespread interest has been agitated in binding protein to solid surfaces because bound proteins were recognized to have extensive applications in emerging environmentally benign catalysis, biomimetic energy conversion, and clinical diagnosis.[1–3] One major challenge frequently encountered in protein binding was how to preserve the active sites from denaturation and ensure the accessibility of active sites as well.[2,4] Most immobilization methods previously reported could effectively retain the active conformation of bound proteins, but could not rationally control the orientation of enzymes.[5,6] A part of active sites might thus be buried and inaccessible, leading to a dramatic decrease in the bioactivity compared with the native enzymes. Few attempts to control the enzymatic orientation through tailoring the wetting properties[7] or surface charges[8] of the supports revealed that the rational artificial interference was not infeasible. However, in the approaches already reported, a reactive terminal tag or a protein conjugate had to be used.[7,8]

Recently, efforts have been made toward the orientated attachment of proteins to solid surfaces through electrostatic assembly.[8–10] The electrostatic recognition strategy is thus believed to be a simple and biocompatible alternative to control the protein orientation. The vital element in the electrostatic-involved approach is to selectively recognize the biomolecules by the predetermined sites of solid surface. Physical-character-alterable ionic supports, such as biomacromolecules,[11,12] charged polymers,[13,14] and inorganic ionic materials[1,15] were proved to be feasible to site-directly recognize proteins. Because of their structural stability, rigidity, and variety, inorganic ionic materials possess considerable advantages in inducing the orientated adsorption of proteins.

As a support facilitating effective and robust electrostatic-induced interfacial recognition, inorganic ionic layered materials have attracted much attention due to their expandable flexible bidimensional spaces. The flexible space was found to be capable of spontaneously matching the guest dimension

Correspondence concerning this article should be addressed to J. He at jinghe@263.net.cn.

© 2010 American Institute of Chemical Engineers

and size, thus facilitating the encapsulation of biomacromolecules than rigid pores.[16,17] Among the layered hosts, layered double hydroxides (LDHs), a kind of biocompatible and low toxic anionic clays,[18] proved efficient in the immobilization of urease enzyme,[19] candida rugosa,[20] and alkaline phosphatase[21] by "soft-chemistry" routes including co-precipitation and anion exchange. The conventional "soft-chemistry" approaches provided tunable but long-term intercalation processes, giving bioactive molecules the chance to change conformation or even to get denatured. An effective alternative to encapsulate biomacromolecules into LDHs has been reported more recently,[22] that was, to restack exfoliated LDH sheets in presence of proteins. However, all the reports paid no attention on the molecule orientation of encapsulated proteins in involving layered materials as inorganic components for electrostatic-driven interfacial assembly.

So, in this article, presented is the first report on controlling lipase orientations via the facile and effective electrostatic-induced interfacial recognition by LDH nanosheets (LDHNSs). The process has proved to be rapid, efficient, and robust, leading to varied PPL orientations depending on the PPL loading. The relationship between the bioactivity and orientation of bound enzymes has been referred to for the first time.

Experimental Section

Materials

Porcine pancreatic lipase (PPL, Type II, as salt free dry powders) from Sigma-Aldrich was used without further purification. Glyceryl triacetate (99%) was from Alfa-Aesar. All other chemicals applied in this work were of analytic grade and used as received. All aqueous solutions were prepared using the deionized and decarbonated water.

Preparation of LDHNSs

The LDH nanosheets (LDHNSs) were prepared by exfoliating the lactate-intercalated LDHs in aqueous medium.[23] The lactate-intercalated LDHs were first synthesized by a co-precipitation method. Typically, 0.20 mol of lactic acid was dissolved by adding 1.25 M NaOH solution until pH = 10. Then a mixture solution of 0.02 mol of magnesium nitrate and 0.01 mol of aluminum nitrate (Mg/Al = 2) in 60 mL of deionized and decarbonated water was added dropwise under vigorous agitation. The resulting slurry was stirred under reflux for 10 h, and then centrifuged. The white solid was washed thoroughly with deionized and decarbonated water.

The wet lactate-intercalated LDHs were suspended into 600 mL of deionized and decarbonated water. The suspension was refluxed under vigorous agitation until a translucent colloidal solution was produced. The exfoliated LDHs were denoted LDH nanosheets (abbreviated as LDHNSs). The content of LDHNSs in the colloidal solution is estimated to be 4 mg/mL. In the whole procedure, an inert atmosphere or sealed container was used to avoid contamination by atmospheric CO_2. The LDHNSs colloidal solution was dropped on a glass slide and vacuumed to dry, producing the restacked sample.

Assembly of PPL with LDHNSs

LDHNSs colloidal solution (1.0 mL) was exposed at 303 K to freshly prepared PPL solution in HCl-tris buffer (pH = 7.5). The PPL concentration was set as 0.0125, 0.025, 0.05, 0.1, 0.2, 0.4, 0.8, 1.0, 1.2, 1.4, 1.6, 1.8, 2.0, 2.2, 2.4, 2.6, 2.8, 3.0 mg/mL, corresponding to an input PPL/LDHNSs mass ratio of 0.125, 0.25, 0.5, 1, 2, 4, 8, 10, 12, 14, 16, 18, 20, 22, 24, 26, 28, and 30 (g/g). The mixture was oscillated in an incubator at 150 rpm for 10 h. The resulting precipitate was centrifuged, washed with fresh buffer to remove the unbound enzyme, and then lyophilized. If not specially indicated, the PPL-LDHNSs hybrids for characterization were all lyophilized powders. The supernatant was collected for measuring the protein content by Bradford method.[24] The protein loading was estimated by subtracting the protein remaining in the supernatant from the initial protein content. The solids are abbreviated as PPL-LDHNSs-n (n represents the mass ratio of PPL to LDHNSs in the resulting PPL-LDHNSs hybrids).

In the measurement of PPL loading as a function of time, different volumes of LDHNSs colloidal solution were suspended in the 30 mg/mL PPL solution in HCl-tris buffer. The mixture was taken at regular intervals to determine the amount of bound protein. For comparison, the similar procedure was adopted for the assembly of PPL with lactate-intercalated LDH.

Characterization

Powder XRD patterns from 3° to 70° were obtained on a Shimadzu XRD-6000 instrument using Cu Kα radiation with a scan rate of 5°/min. The XRD patterns from 0.5° to 5° were taken on a Hitachi D/MAX-2500 instrument using Cu Kα radiation, and a scan rate of 0.5°/min. AFM images were taken on a Digital Instruments NanoScope IV atomic force microscopy in tapping-mode using a Si tip cantilever with a force constant of 20 N/cm. The LDHNSs colloidal solution was deposited on Si wafer and lyophilized. The zeta potential was measured on a Malvern Zetasizer Nano ZS zeta potential analyzer. FTIR spectra were recorded on a Bruker Vector 22 spectrometer with 60 scans at 4 cm^{-1} resolution using standard KBr disk method. The attenuated total reflectance (ATR) FT-IR experiments were conducted on a Nicolet Nexus 470 spectrometer configured with a Smart OMNI sample accessory. PPL or PPL-LDHNSs powders were spread onto the Ge ATR accessory, and the spectra were collected at 4 cm^{-1} resolution in the absorption mode by 256 scans. High resolution TEM (HRTEM) images were taken on a JEOL JEM-2010 electron microscope operating at 200 kV. The specimen was ultrasonically dispersed in ethanol medium, and dropped on a holey ultrathin carbon film. The morphologies of LDHNSs and PPL-LDHNSs were observed on a Hitachi S-4700 field emission SEM (FESEM). The droplet size distribution of glyceryl triacetate in water was measured on a Mastersizer 2000 laser particle size analyzer. To exclude the disturbance of the large LDHNSs particles on the microemulsion droplets, the PPL-LDHNSs particles were removed with ultrafiltration membrane from the mixture in prior to measurements.

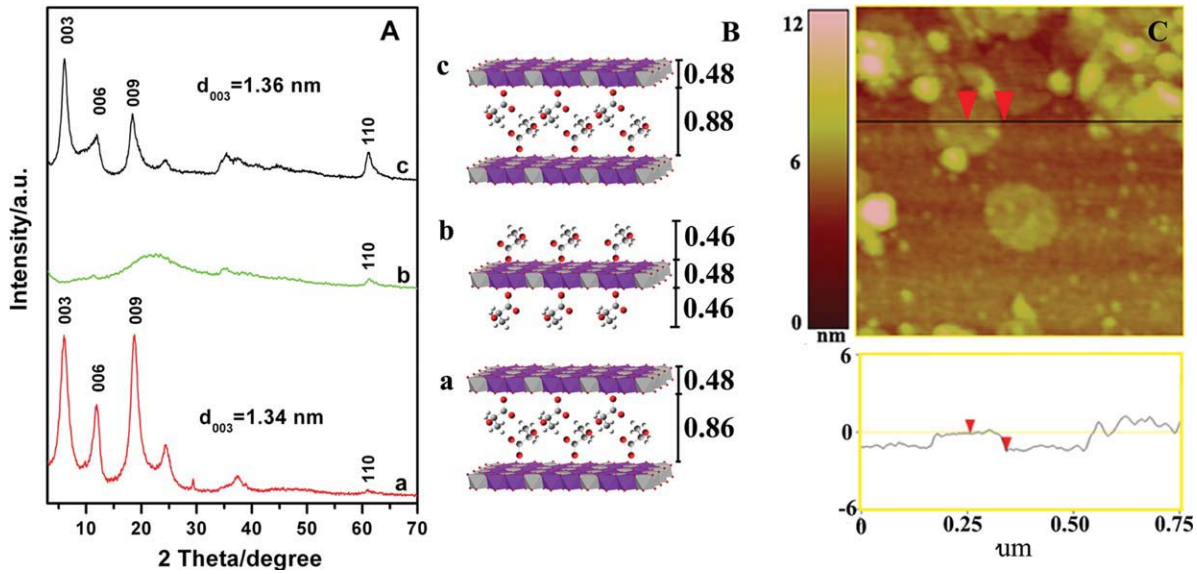

Figure 1. (A) XRD patterns and (B) schematic structural illustration of lactate-intercalated LDHs (a), LDHNSs (b) and restacked LDHs (c).

The purple part in the layers represents $Mg(OH)_6$ octahedra and the grey one represents the $Al(OH)_6$ octahedra. (C) Tapping-mode AFM image of LDHNSs deposited on a Si wafer substrate, with a height profile along the marked line. [Color figure can be viewed in the online issue, which is available at wileyonlinelibrary.com.]

Activity assays

The hydrolytic activity of soluble PPL or PPL-LDHNSs nanohybrids was determined at 303 K by titrating (with aqueous NaOH) the acetic acid produced in the hydrolysis of glyceryl triacetate.[25] Typically, 25 g of glyceryl triacetate was dispersed in HCl-tris buffer (pH = 7.5) under vigorous shaking, which was finally made up to a volume of 500 mL, giving a translucent mixture solution. The droplet size of glyceryl triacetate in water was measured as ~60 nm. After an aliquot (40 mL) was placed in a bath at 303 K for 5 min, soluble PPL or PPL-LDHNSs (amounting to the same amount of pristine PPL) in 15 mL of HCl-tris buffer was added. In 30 min, 30 mL of anhydrous alcohol was added to terminate the reaction. The mixture was titrated with 0.05 M NaOH solution until pH = 8. The pH value was monitored by a pH meter. Control assays were performed following the same procedure to exclude the NaOH consumption by pristine buffer, LDHNSs suspension, and glyceryl triacetate solution.

To determine the thermal stability of enzymatic activity, soluble PPL or PPL-LDHNSs was exposed to thermal treatment respectively at 303, 313, 323, 333, 343, 353, 363, and 373 K for 1 h. Then the active assays were carried out following the above procedure.

Results and Discussion

Preparation of LDHNSs

The XRD patterns of lactate-intercalated LDHs, LDHNSs and restacked LDHs are shown in Figure 1A. The lactate-intercalated Mg_2Al-LDH (before exfoliation) shows a sharp basal reflection at 5.98° arising from (003) plane, with a basal spacing of 1.34 nm. The basal spacing corresponds to an interdigitated bilayer arrangement of lactate anions within the interlayer galleries, consistent with reported previously.[26] The exfoliation causes the complete disappearance of (00*l*) reflections characteristic of the ordered structure in the layer-stacking direction. Instead, a broad reflection typical of a random aggregation of exfoliated LDH sheets[27,28] is observed at 20–30°. The (110) reflection at 61.20°, originating from the LDH layers, is well retained. The restacked LDH displays similar XRD pattern to its precursor (before exfoliation). That means, the LDHNSs prepared here have well retained the two-dimensional layered structure without any destruction, and have the ability to restack into ordered layer arrays in proper conditions with the environmental anions intercalation. Figure 1B gives the schematic structure of lactate-intercalated LDHs, LDHNSs, and restacked LDHs, respectively.

Figure 1C illustrates the tapping mode AFM image of the LDHNSs with the height profile along the marked line. Single thin sheets of LDHNSs are observed in 170–190 nm size, accompanied with smaller fragments and sheet overlapping. The height profile measurement indicates the sheet thickness is uniformly ca. 1.4 nm, which corresponds to the thickness of one single LDH layer plus two-sided flat monolayer lactate arrangement (Figure 1B). The zeta potential measurement indicates the LDHNSs plus bound lactate ions are positively charged in 28.8 mV, which could facilitate the assembly with other environmental anions. The environmental anions can react with the LDHNSs through electrostatic force and are also likely to simultaneously substitute the previous lactate anions.

Interfacial assembly of PPL with LDHNSs

PPL (pI = 5.0), well recognized as clubbed protein with a three dimensional size of 4.6 × 2.6 × 1.1 nm^3 and widely applied in biocatalytic reactions,[29,30] has been used as model

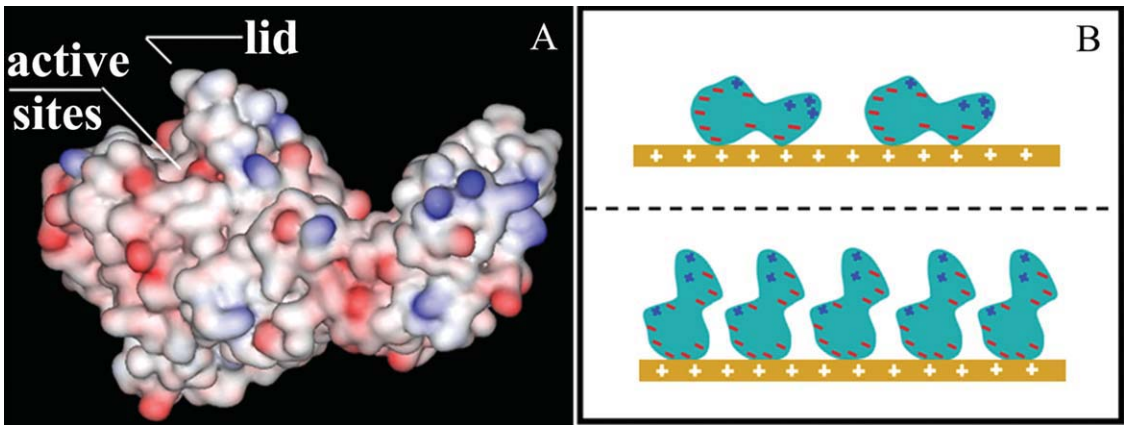

Figure 2. (A) Electrostatic surface potential for PPL at pH 7.5 produced by GRASP II (Dr. Honig's Lab, Columbia University) and colored according to the electrostatic potential (negatively charged regions are shown in red and positively in blue); (B) schematic representations showing two possible molecular orientations of PPL immobilized onto the positively charged LDHNSs.

[Color figure can be viewed in the online issue, which is available at wileyonlinelibrary.com.]

enzyme in this study. The catalytic active sites of PPL are composed of Ser 152, Asp 176, and His 263 residues, located near the hydrophobic loop consisting of a flexible short-one-turn helix.[31] As shown in Figure 2A, for PPL at pH 7.5, the negatively charged domains, supposedly providing a strong affinity to positively charged LDHNSs, are visualized on the side opposite to the active sites. The net negative charge per PPL molecule at pH 7.5 is estimated to be -12.85 (an electron $= 1.6 \times 10^{-19}$ C) based on the zeta potential measurement, using bovine serum albumin (BSA) and lysozyme as references. The zeta potentials for PPL, BSA, and lysozyme are measured to be -1.67 mV, -2.19 mV, and $+1.06$ mV. The charge for BSA and lysozyme has been reported to be -17[32] and $+8$.[33] With its negative-charge concentrated domains most adjacent to the positively charged LDHNSs, PPL is preferably orientated to lie flat on the LDHNSs surface (Figure 2B) at low PPL loading. At low PPL loading, only a part of lactates are substituted by PPL. The projective area of one PPL on the LDH layer is relatively large because of the bulky dimension of PPL molecules. Because of the electrostatic attraction of LDHNSs to PPL and as well the hydrophobic affinity between PPL molecules, the gradual replacement of lactate by PPL is supposed to occur to its ultimate extension. With more lactate anions replaced, the projective area held by one PPL has to be reduced by changing the PPL orientation (flat to upstanding, Figure 2B) or even conformation (unfolding for example). In this case of orientation adaptation, a considerable adsorption capacity can be expected. The orientation alteration has been previously observed for Lysozyme.[34]

Figure 3A shows the initial adsorption amount of PPL on LDHNSs, varying with the input mass ratio of PPL to LDHNSs. The adsorption on lactate-intercalated LDHs is also performed and displayed for comparison. From the initial adsorption amount, which is defined as the percentage of the bound PPL in the total input PPL dosage in the initial 10 min, it could be found that PPL is assembled with LDHNSs much faster than with lactate-intercalated LDHs. On the LDHNSs, PPL is adsorbed completely in 10 min without free PPL remaining in the solution until the input dosage equals 10/1 (g/g, PPL/LDHNSs). On the lactate-intercalated LDHs, however, the initial adsorption amount has decreased to 64% at an input dosage of 1/1, which is even slightly lower than the adsorption amount (66%) on LDHNSs at an input dosage of 30/1. The results reveal that the assembly process of PPL on LDHNSs is considerably rapid and the assembly amount of PPL is impressively high. The steady or quasi-steady state for the assembly of PPL with LDHNSs is achieved in 10 h.

Figure 3B shows the adsorption isotherms (Q_e–C_e profile) of PPL on LDHNSs and on lact-intercalated LDHs. Wherein, Q_e represents the gram of bound PPL on per gram LDHNSs and C_e stands for the PPL concentration remaining in solution after assembly.[24] The adsorption isotherm of PPL on LDHNSs displays a typical "S" shape. Q_e first increases gradually with C_e, then shows a sharp increase, and finally reaches a plateau. The leaching experiment carried out by oscillating the PPL-LDHNSs solid in a buffer solution excludes the possibility of protein aggregation. Almost no PPL leaching from the solid was observed, as was evidenced by a PPL content of less than 0.1% detected in the supernatant. The sharp increase of Q_e thus confirms the previous assumption of the PPL orientation alteration from flat to vertical. For the limited charge density of LDH layer, the layer unit area occupied by one PPL molecule is required to reduce with increasing PPL loading. The quantitative discussion to confirm the PPL orientation alteration will be given later based on the combination of adsorption isotherm and XRD results. No soluble PPL remains free when PPL loadings are lower than 10, which is in accordance with Figure 3A. For the PPL adsorption on lact-intercalated LDHs however, a typical L-shape isotherm has been observed, showing a saturation adsorption amount of 9.92 g/g. This is not surprising because it is difficult for bulky PPL to replace the lactate anions intercalated in the LDH interlayer galleries.

The assembly of PPL with LDHNSs is monitored by the FTIR spectroscopy. The spectra for PPL-LDHNSs with increasing PPL proportion are shown in Figure 4. The

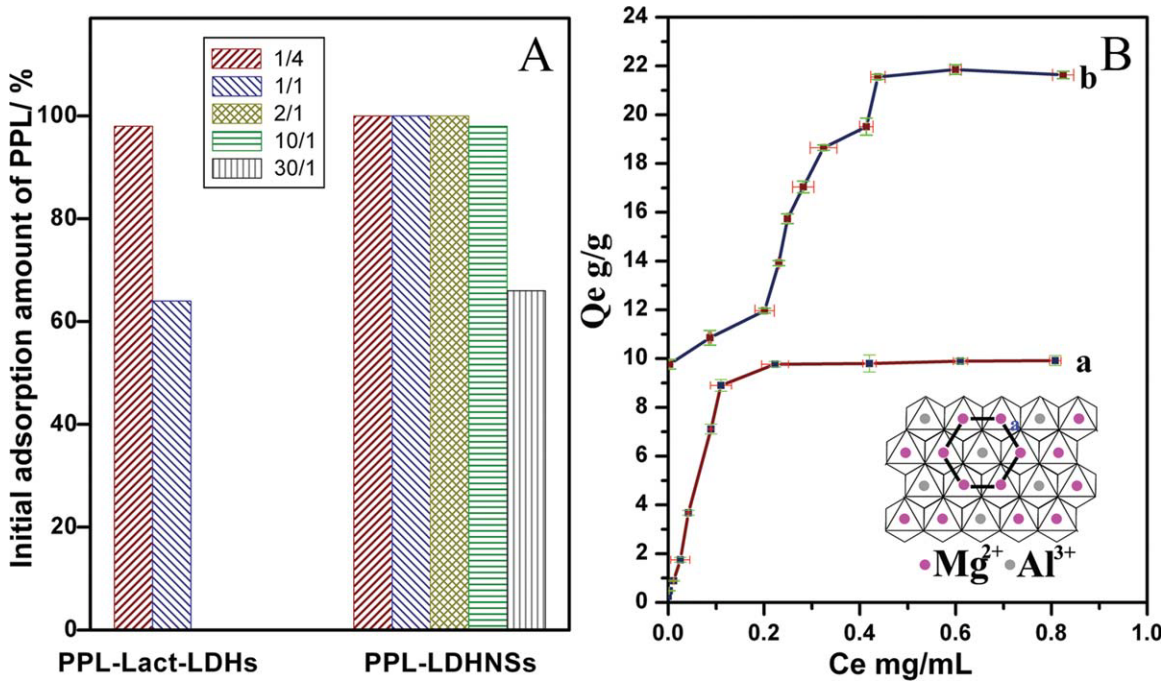

Figure 3. (A) Initial adsorption amount of PPL assembled with LDHNSs and lactate-intercalated LDHs; (B) the adsorption isotherm of PPL on LDHNSs (a) and on lactate-intercalated LDHs (b) (Q_e~C_e profile.

Q_e: PPL in gram on per gram LDHNSs, C_e: the steady concentration of PPL in buffer solution after assembly). The data were reported as the average of two reproducible experiments. The errors for Q_e and C_e are given. Inset: the schematic illustration of the atomic structure of the LDHNSs layer. [Color figure can be viewed in the online issue, which is available at wileyonlinelibrary.com.]

absorption bands of carboxylate at 1385 cm^{-1} and —C-OH moiety at 1120 cm^{-1} of lactate anions decrease in intensity with increasing PPL loading and finally could hardly be resolved at PPL/LDHNSs = 9. The absorption at 1055 cm^{-1}, associated with the —C—OH groups of lactate anions, also gradually decrease along with increased PPL loadings. The replacement of lactate by PPL could be better interpreted by the quantitative results in Table 1. In the quantitative analysis, the band at 446 cm^{-1} assigned to the vibration of $[AlO_6]^{3-}$ group and Al—O bond is used as the internal standard, which has been reported to be invariable for Mg/Al-LDHs intercalated with different anions.[35] The band at 1385 cm^{-1} associated with carboxylate of the lactate is employed to determine the lactate content. For PPL-LDHNSs-9 and PPL-LDHNSs-13, the band at 1385 cm^{-1} was fitted by OriginPro 7.0 in the Gaussian mode. The data in Table 1 clearly reveal the gradual decrease of lactate content along with increasing PPL loading.

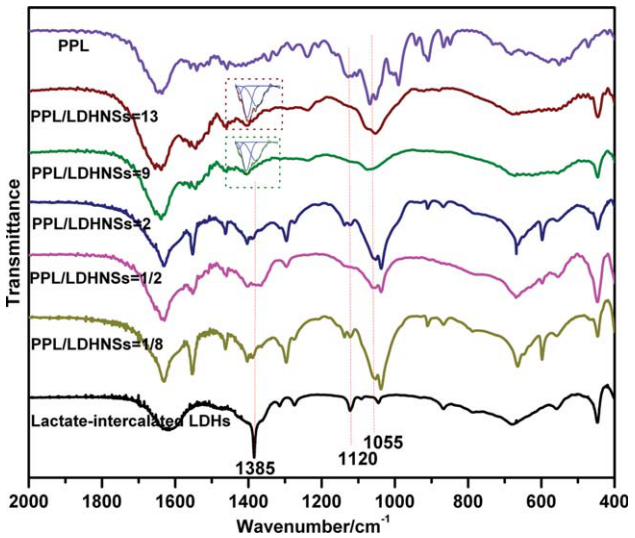

Figure 4. (A) FTIR spectra of lactate-intercalated LDHs, PPL-LDHNSs with different PPL loadings, and pristine PPL powder.

Inset: the magnification of the band at 1385 cm^{-1} fitted by OriginPro 7.0 in the Gaussian mode for PPL-LDHNSs-9 and PPL-LDHNSs-13. [Color figure can be viewed in the online issue, which is available at wileyonlinelibrary.com.]

Characterization of PPL-LDHNSs nanohybrids

The structures of PPL-LDHNSs nanohybrids are studied by XRD and TEM techniques. The HRTEM images of PPL-

Table 1. Quantitative Analysis Data of the Lactate Content on Lact-LDH and PPL-LDHNSs-n from the FTIR Spectra

Sample	Corrected Band Area (A) 445 cm^{-1}	Corrected Band Area (A) 1385 cm^{-1}	A_{1385}/A_{445}	Lactate Content (%)
Lact-LDH	1.279	2.466	1.928	100
PPL-LDHNSs-0.125	0.922	1.711	1.856	96.3
PPL-LDHNSs-0.5	2.102	1.295	1.623	84.2
PPL-LDHNSs-2	0.611	0.771	1.262	65.5
PPL-LDHNSs-9	0.708	0.177*	0.250	13.0
PPL-LDHNSs-13	0.835	0.173*	0.207	10.7

*The band at 1385 cm^{-1} was fitted by OriginPro 7.0 in the Gaussian mode.

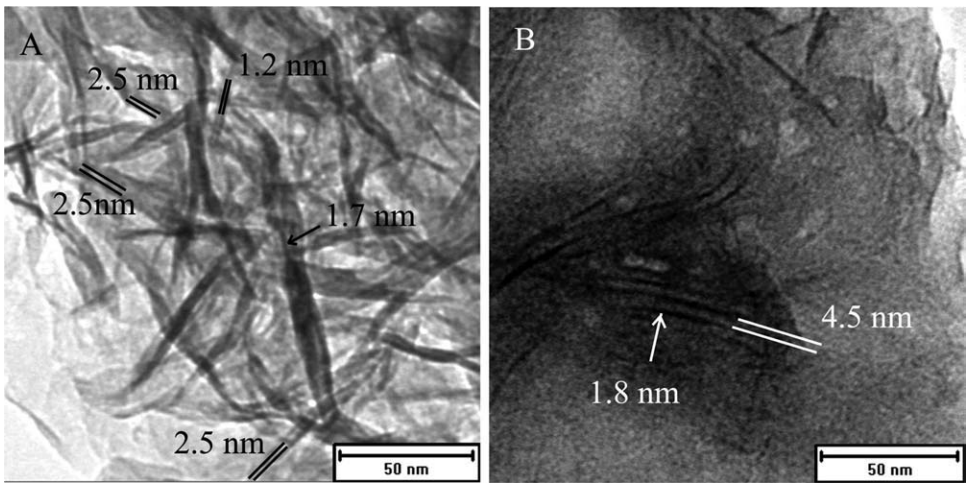

Figure 5. HRTEM images of PPL-LDHNSs-0.5 (A) and PPL-LDHNSs-13 (B).

LDHNSs-0.5 and PPL-LDHNSs-13 are shown in Figure 5. The layer-stacking architectures are clearly presented for the both PPL-LDHNSs nanohybrids. The interlayer spacing of 2.5 nm resolved for PPL-LDHNSs-0.5 (Figure 5A), approximately matches one dimensional size of PPL (2.6 nm). The coexisting interlayer spacing of 1.2 nm is in accordance with another dimensional size of PPL (1.1 nm). However, the lamellas restacking through PPL induction are quite thin in thickness, no long-range well-ordered pillared structures evidently observed. For PPL-LDHNSs-13, well-ordered pillared structure with an interlayer spacing of 4.5 nm could be observed (Figure 5B), corresponding to the third dimensional size of PPL (4.6 nm). The HRTEM observation demonstrates the PPL orientations (Figure 2B): lying flat and upstanding, also well accounting for the steep increase in the Q_e–C_e profile (Figure 3B). The thickness of LDH slabs is estimated to be ca. 1.7 or 1.8 nm in HRTEM images, which is much larger than the thickness of single LDH layer (0.48 nm).[36]

The layer-stacking architectures of PPL-LDHNSs-0.5 and PPL-LDHNSs-13 could also be rationally deduced from the XRD patterns shown in Figure 6. For PPL-LDHNSs-0.5 (Figure 6A), a broad basal reflection appears at 1.69° with a basal spacing (d_{003}) of 2.91 nm, which corresponds to the PPL size of 2.6 nm in one dimension. Similar to the HRTEM measurement, an additional basal reflection at 2.89° is also detected with the d_{003} = 1.61 nm, corresponding to another PPL dimensional size of 1.1 nm. Yet the layer stacking induced by PPL, bulky in dimension and insufficient in input quantity, is not ordered well enough, showing weak basal reflections. For PPL-LDHNSs-13 (Figure 6B), the basal spacing (d_{003}) is 5.13 nm, related to the PPL dimensional size of 4.6 nm. Meanwhile, the wide-angle XRD pattern of

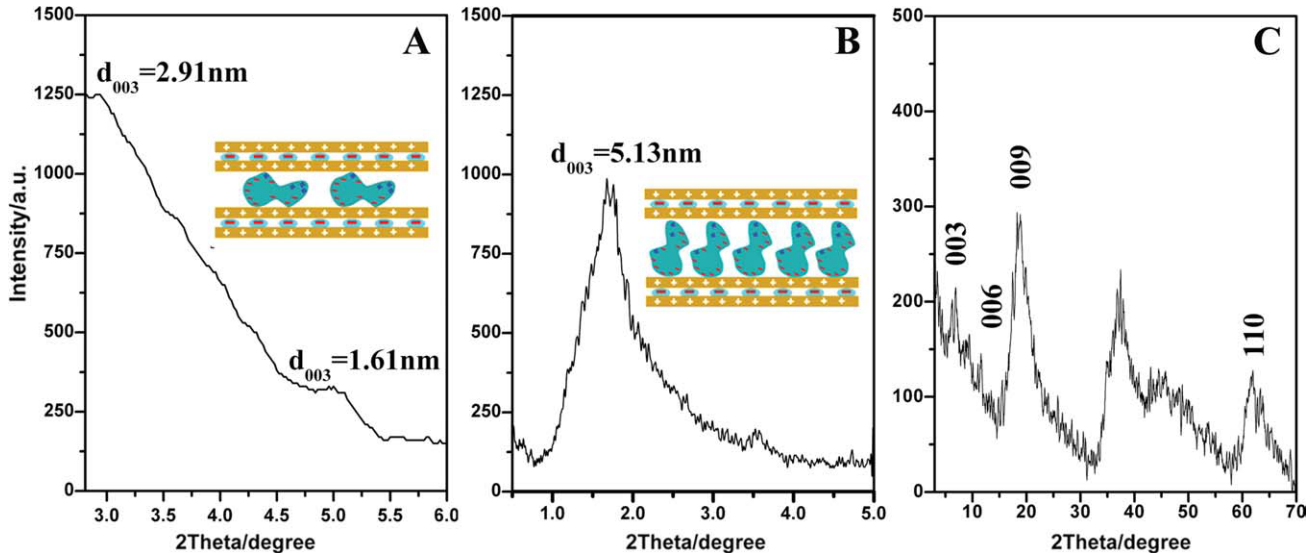

Figure 6. XRD patterns at low angle of PPL-LDHNSs-0.5 (A) and PPL-LDHNSs-13 (B); (C) wide-angle XRD pattern of PPL-LDHNSs-0.5.

Inset: schematic representations of the pillared layered structures. [Color figure can be viewed in the online issue, which is available at wileyonlinelibrary.com.]

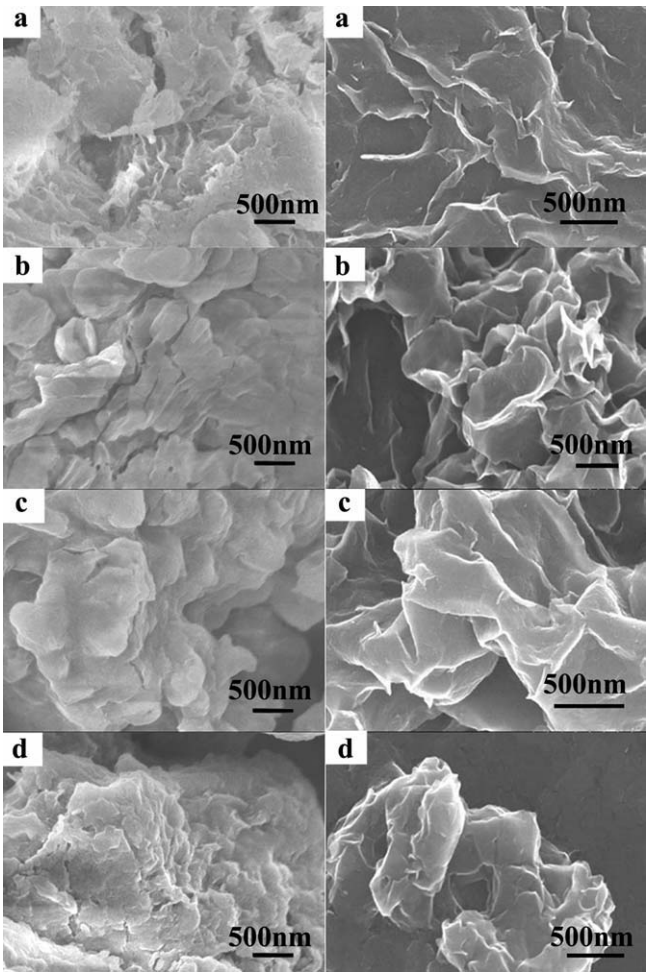

Figure 7. FESEM images of LDHNSs (a), PPL-LDHNSs-0.125 (b), PPL-LDHNSs-0.5 (c), and PPL-LDHNSs-4 (d) dried by lyophilization (left) and solvent-evaporation under vacuum (right).

PPL-LDHNSs-0.5 (Figure 6C) shows weak diffraction of lactate-intercalated LDHs, in accordance with the presence of lactate anion revealed in Table 1 as well. The lactate-intercalated phase accounts for the slab thickness of ca. 1.7–1.8 nm observed in Figure 5. A restacked structure consisting of two LDH layers (2×0.48 nm[36]) and an interdigitated bilayer of the intercalated lactate (0.86 nm[26]) has a slab thickness of 1.82 nm. PPL-LDHNSs hybrids, therefore, have proved to have a layer-stacking architecture resembling second-staging[37,38] structure, as schematically illustrated in the insets for Figures 6A,B.

On the basis of the XRD and adsorption results, the PPL orientation at high PPL loading can be well understood quantitatively. As observed in the adsorption isotherm, Q_e reaches 21.6 g/g at saturation. The molar ratio of Al^{3+} in LDHNSs to PPL is thus calculated to be 18.2/1. That is, 1/18.2 PPL molecule is adsorbed on per charge site of LDHNSs. For the Mg_2Al-LDHNSs prepared in this work, the lattice parameter a, defined as the mean distance between adjacent Mg centers in the close-packed sheets parallel to the plane (Figure 3B inset), is calculated as 0.3035 nm ($2d_{110}$) here. As shown in the inset of Figure 3B, the unit area for one charge site on LDH layer could be calculated as 0.2394 nm^2. Thus at saturation, the average projective area of one single PPL on the LDH slab is about 4.3451 nm^2, excluding the possible arrangement of PPL with its maximal dimension paralleling LDH slab, consistent with a basal spacing of 5.13 nm as well.

Further, in light of the results of XRD pattern, adsorption isotherm, and AFM image, the origin of lactate anion resolved in the FT-IR quantitative analysis could be revealed. The PPL number at saturation adsorption is calculated to be 6.5×10^3 per single LDHNS. The negative net charge for one PPL anion at pH 7.5 has been measured as 12.85 eV. The total negative charge of all PPL on per LDHNSs is thus calculated to be 8.3×10^4 eV. For the LDHNSs layer, the positive charge density σ could be calculated using Eq. 1;

$$\sigma = \frac{x}{a^2 \bullet \sin\theta} \tag{1}$$

wherein x is the molar ratio of Al in total metal content, and θ is the angle for the lattice parameters a and b. Herein, x is calculated as 0.3333, and θ is 60°. Thus, σ is calculated to be 4.1774 eV/nm^2. For the LDHNSs with an average of ~180 nm along *ab*-plane direction, the total positive net charge is calculated as 8.8×10^4 eV, slightly higher than the total negative charge of all PPL on per LDHNSs (8.3×10^4 eV). So, besides the lactates in the second-staging structure, trace of lactates is also present as co-existing anion with PPL to completely balance the LDHNSs charge.

The morphologies of LDHNSs and PPL-LDHNSs are investigated by FESEM (Figure 7). For lyophilized PPL-LDHNSs, the plate-like stacking is clearly observed, and the lamella curliness gets less visible than lyophilized LDHNSs. For the PPL-LDHNSs dried by solvent-evaporation under vacuum, the curled degree of LDH edges becomes more distinct than the LDHNSs counterpart. The morphology variations due to the PPL presence and the dryness approaches suggest that, not only the LDHNSs could orientate PPL molecules, but also the adsorbed PPL could induce the flexibility of thin flake-like LDHNSs.

Conformation and bioactivity of bound PPL

Table 2 provides a comparison of the secondary structure features of pristine and bound PPL by analyzing their ATR-

Table 2. Peak Position and Component Assignment of Amide I in the ATR-FTIR Spectra

Sample	Peak Position (cm^{-1})*	Assignment	Content (%)
PPL	1632	β-sheet	17
	1642	Random coil	17
	1650	α-helix	10
	1659, 1667, 1673, 1680	β-turn	40
PPL-LDHNSs-0.5	1632	β-sheet	17
	1642	Random coil	15
	1650	α-helix	11
	1659, 1667, 1673, 1680	β-turn	42
PPL-LDHNSs-13	1632	β-sheet	19
	1642	Random coil	15
	1650	α-helix	9
	1659, 1667, 1673, 1679	β-turn	41

*The Gaussian curve-fitting of the spectra in the amide I region.

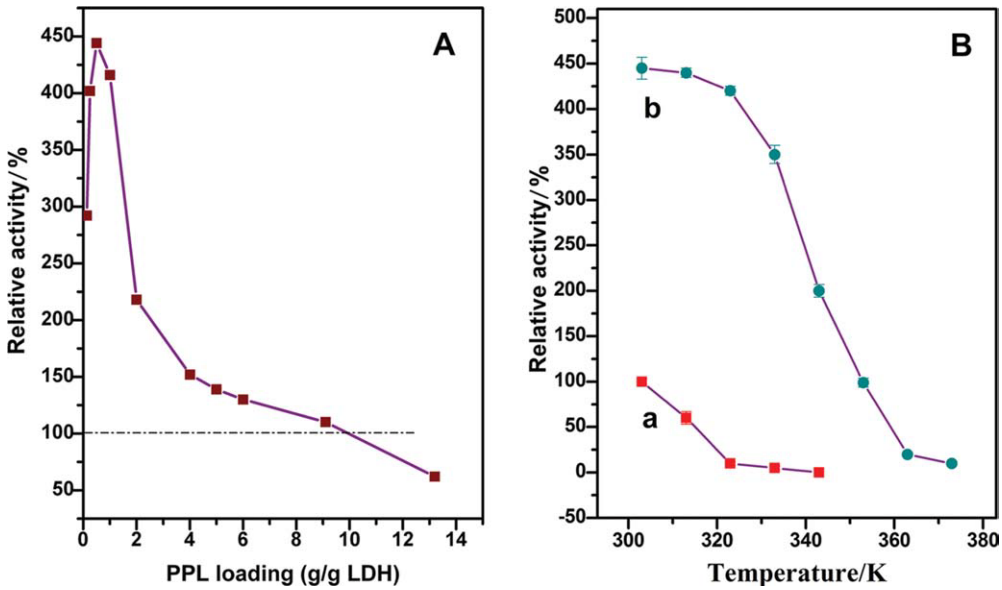

Figure 8. (A) Dependence of the PPL-LDHNSs activity in the hydrolysis of glyceryl triacetate on the PPL loading; (B) dependence of relative activity of PPL (a) and PPL-LDHNSs-0.5 (b) on the thermal treatment temperature.

[Color figure can be viewed in the online issue, which is available at wileyonlinelibrary.com.]

FTIR spectra in the amide I region from 1600 to 1700 cm^{-1} (largely C=O stretching vibrations of peptide linkages[39]). The absorption bands at 1631–1633, 1642–1643, 1650–1651, and 1659–1680 cm^{-1} are respectively assigned to the components of β-sheets, random coil, α-helix, and β-turns according to previous report.[40] It can be seen from Table 2 that the contents of these basic components in PPL-LDHNSs-0.5 and PPL-LDHNSs-13 are almost consistent with pristine PPL, indicative of the complete preservation of PPL active conformation in the electrostatic-induced interfacial assembly with LDHNSs. It is confirmed that, in the interfacial adsorption, what has changed is only the PPL orientation rather than protein conformation.

As can be seen from Figure 8A, in the hydrolysis of glyceryl triacetate, the catalytic activity of the PPL-LDHNSs hybrids with a PPL loading of lower than 9 is remarkably enhanced in comparison with their soluble counterpart. The relative activity reaches a maximum (445%) for PPL-LDHNSs-0.5. Concerning the reason for the dramatic bioactivity enhancement of adsorbed PPL, one might readily think of the emulsifying characteristics of LDHNSs nanoparticles, just as in the "Pickering emulsions". So the droplet size of glyceryl triacetate in water was investigated in this work. It is found that the droplet size of glyceryl triacetate in water is distributed around 60 nm (Figure 9A), much smaller than the LDHNSs size (~180 nm). So this possibility could be excluded. However, the LDHNSs particles are found to play a role at the oil/water interface in another way. The droplet size of glyceryl triacetate in water holds around 60 nm and is not influenced by the presence of soluble PPL in the 120 min measurement (Figure 9A). The introduction of PPL-LDHNSs-0.5, however, decreases the droplet size to ~45 nm in 30 min (Figure 9B). This is proposed to be one reason for the enhanced bioactivity.

Still, the PPL orientations may also play a critical role in improving the catalytic activity. With PPL/LDHNSs lower than 9, PPL molecules are orientated flat with the active

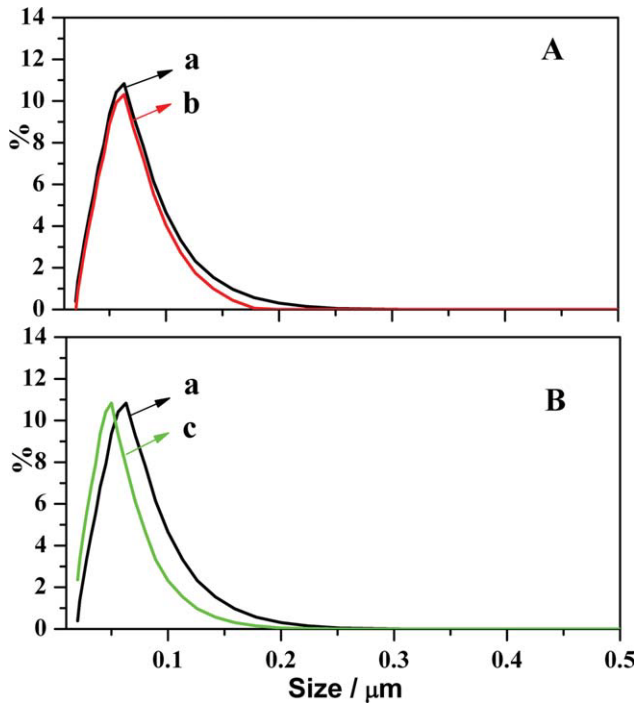

Figure 9. The size distribution of glyceryl triacetate in water in the presence of (A) soluble PPL, and (B) PPL-LDHNSs-0.5 in (a) 0 h, (b) 2.0 h, and (c) 0.5 h.

[Color figure can be viewed in the online issue, which is available at wileyonlinelibrary.com.]

sites facing to the LDH hydrated layers. The hydrogen-bonding environment neighboring the active sites might favor the biologic functioning of PPL. The active sites of PPL in the less ordered restacked architecture are additionally accessible more readily to the substrate, which might also be one reason. For PPL-LDHNSs-13, however, the upstanding PPL in high loading are arranged densely like protein aggregates and the active site thus faces another neighboring PPL.

The enhancement of the thermal stability for the PPL-LDHNSs is also observed. Figure 8B shows typical thermal denaturation curves of PPL and PPL-LDHNSs-0.5. The apparent unfolding transition midpoint, T_m, increases from ca. 323 K for pristine PPL to 364 K for PPL-LDHNSs-0.5.

Conclusion

In summary, we have demonstrated clearly that the PPL orientation in the confined interlayer space of LDHs could be effectively controlled by varying the enzyme loadings in the elecrostatic-induced assembly with LDHNSs. The significance of this strategy lies in its simplicity, rapidness, and robustness, as well as improvement of the bio-activity. This might help developing a general method for orientation-controlled immobilization of proteins to perform molecular recognition experiments and be potentially useful in the preparation of the protein microarray nanodevices.

Acknowledgments

The authors thank the financial support from NSFC, Program for Changjiang Scholars and Innovative Research Team in University (IRT0406), project 111 (B07004), and 973 project (2009CB939802).

Literature Cited

1. Niemeyer CM. Nanoparticles, proteins, and nucleic acids: biotechnology meets materials science. *Angew Chem Int Ed*. 2001;40:4128–4158.
2. Bornscheuer UT. Immobilizing enzymes: how to create more suitable biocatalysts. *Angew Chem Int Ed*. 2003;42:3336–3337.
3. Cao L. Immobilised enzymes: science or art? *Curr Opin Struct Biol*. 2005;9:217–226.
4. Edmiston PL, Lee JE, Cheng SS, Saavedra SS. Molecular orientation distributions in protein films. I. Cytochrome *c* adsorbed to substrates of variable surface chemistry. *J Am Chem Soc*. 1997;119:560–570.
5. Mao H, Yang T, Cremer PS. Design and characterization of immobilized enzymes in microfluidic systems. *Anal Chem*. 2002;74:379–385.
6. DeLouise LA, Miller BL. Quantitative assessment of enzyme immobilization capacity in porous silicon. *Anal Chem*. 2004;76:6915–6920.
7. Wannerberger K, Welin-Klintström S, Arnebrant T. Activity and adsorption of lipase from *humicola lanuginosa* on surfaces with different wettabilities. *Langmuir*. 1997;13:784–790.
8. Wang X, Zhou D, Sinniah K, Clarke C, Birch L, Li H, Rayment T, Abell C. Electrostatic orientation of enzymes on surfaces for ligand screening probed by force spectroscopy. *Langmuir*. 2006;22:887–892.
9. MacBeath G, Schreiber SL. Printing proteins as microarrays for high-throughput function determination. *Science*. 2000;289:1760–1763.
10. Hong R, Fisher NO, Verma A, Goodman CM, Emrick T, Rotello VM. Control of protein structure and function through surface recognition by tailored nanoparticle scaffolds. *J Am Chem Soc*. 2004;126:739–743.
11. Schirmer EB, Carta G. Protein adsorption kinetics in charged agarose gels: effect of agarose content and modeling. *AIChE J*. 2009;55:331–341.
12. Schirmer EB, Carta G. Protein adsorption in charged agarose gels studied by light microscopy. *AIChE J*. 2007;53:1472–1482.
13. Kim J, Kosto TJ II, Manimala JC, Nauman EB, Dordick JS. Preparation of enzyme-in-polymer composites with high activity and stability. *AIChE J*. 2001;47:240–244.
14. Russell SM, Carta G. Multicomponent protein adsorption in supported cationic polyacrylamide hydrogels, *AIChE J*. 2005;51:2469–2480.
15. Niemeyer CM. Functional hybrid devices of proteins and inorganic nanoparticles, *Angew Chem Int Ed*. 2003;42:5796–5800.
16. Hartmann M. Ordered mesoporous materials for bioadsorption and biocatalysis. *Chem Mater*. 2005;17:4577–4593.
17. Karajanagi SS, Vertegel AA, Kane RS, Dordick JS. Structure and function of enzymes adsorbed onto single-walled carbon nanotubes. *Langmuir*. 2004;20:11594–11599.
18. Choi S-J, Oh J-M, Choy J-H. Human-related application and nanotoxicology of inorganic particles: complementary aspects. *J Mater Chem*. 2008;18:615–620.
19. Vial S, Ghanbaja J, Forano C. Precipitation of Zn_2Al LDH by urease enzyme. *Chem Commun*. 2006;290–292.
20. Rahman MBA, Zaidan UH, Basri M, Hussein MZ, Rahman RNZRA, Salleh AB. Enzymatic synthesis of methyl adipate ester using lipase from *Candida rugosa* immobilised on Mg, Zn and Ni of layered double hydroxides (LDHs). *J Mol Catal B*. 2008;50:33–39.
21. Geraud E, Prevot V, Forano C, Mousty C. Spongy gel-like layered double hydroxide-alkaline phosphatase nanohybrid as a biosensing material. *Chem Commun*. 2008;1554–1556.
22. Chen X, Fu C, Wang Y, Yang W, Evans DG. Direct electrochemistry and electrocatalysis based on a film of horseradish peroxidase intercalated into Ni-Al layered double hydroxide nanosheets. *Biosensor Bioelectron*. 2008;24:356–361.
23. Hibino T, Kobayashi M. Delamination of layered double hydroxides in water. *J Mater Chem*. 2005;15:653–656.
24. Verger R, Sarda L, Desnuelle P. On the sulfhydryl groups of porcine pancreatic lipase and their possible role in the activity of the enzyme, *Biochim Biophys Acta*. 1971;242:580–592.
25. Sharma R, Chisti Y, Banerjee UC. Production, purification, characterization, and applications of lipases. *Biotechnol Adv*. 2001;19:627–662.
26. Newman SP, Cristina TD, Coveney PV, Jones W. Molecular dynamics simulation of cationic and anionic clays containing amino acids. *Langmuir*. 2002;18:2933–2939.
27. Li L, Ma R, Ebina Y, Iyi N, Sasaki T. Positively charged nanosheets derived via total delamination of layered double hydroxides. *Chem Mater*. 2005;17:4386–4391.
28. Liu Z, Ma R, Osasa M, Iyi N, Ebina Y, Takada K, Sasaki T. Synthesis, anion exchange, and delamination of Co-Al layered double hydroxide: assembly of the exfoliated nanosheet/polyanion composite films and magneto-optical studies. *J Am Chem Soc*. 2006;128:4872–4880.
29. Fournet B, Leroy Y, Děcaro J, Rovery M, Kuik JA, Vliegenthart JFG. Primary structure of the glycans of porcine pancreatic lipase. *Eur J Biochem*. 1987;170:369–371.
30. Schmid RD, Verger R. Lipases: interfacial enzymes with attractive applications. *Angew Chem Int Ed*. 1998;37:1608–1633.
31. Borreguero I, Sánchez-Montero JM, Sinisterra JV, Rumbero A, Hermoso JA, Alcántara AR. Regioselective resolution of 1,n-diols catalysed by lipases: a rational explanation of the enzymatic selectivity. *J Mol Catal B*. 2001;11:1013–1024.
32. Shi Q, Zhou Y, Sun Y. Influence of pH and ionic strength on the steric mass-action model parameters around the isoelectric point of protein. *Biotechnol Prog*. 2005;21:516–523.
33. States DJ, Karplus MUK. A model for electrostatic effects in proteins. *J Mol Biol*. 1987;197:122–130.
34. Daly SM, Przybycien TM, Tilton RD. Coverage-dependent orientation of lysozyme adsorbed on silica. *Langmuir*. 2003;19:3848–3857.
35. Kagunya W, Baddour-Hadjean R, Kooli F, Jones W. Vibrational modes in layered double hydroxides and their calcined derivatives. *Chem Phys*. 1998;236:225.

36. Evans DG, Slade RCT. Structural aspects of layered double hydroxides. *Struct Bond*. 2006;119:1–87.
37. Williams GR, O'Hare D. Factors influencing staging during anion-exchange intercalation into $[LiAl_2(OH)_6]X{\cdot}mH_2O$ ($X{=}Cl^-$, Br^-, NO_3^-). *Chem Mater*. 2005;17:2632–2640.
38. Feng YJ, Williams GR, Leroux F, Taviot-Gueho C, O'Hare D. Selective anion-exchange properties of second-stage layered double hydroxide heterostructures. *Chem Mater*. 2006;18:4312–4318.
39. He P, Hu N, Zhou G. Assembly of electroactive layer-by-layer films of hemoglobin and polycationic poly(diallyldimethylammonium). *Biomacromolecules*. 2002;3:139–146.
40. Secundo F, Barletta GL, Dumitriu E, Carrea G. Can an inactivating agent increase enzyme activity in organic solvent? Effects of 18-Crown-6 on lipase activity, enantioselectivity, and conformation. *Biotechnol Bioeng*. 2007;97:12–18.

Manuscript received Jan. 22, 2009, and revision received Oct. 22, 2009.